First-principles study of Adsorption and Gas Sensing Properties of Pt-modified InN for SF₆ Decomposition Components

Youjun Yue,[1] Guilin Chen,[1] Dongyue Wu,[1*] Linxi Zhou,[2] and Yiliduosi Zupaer[1]

[1]Tianjin Key Laboratory of New Energy Power Conversion, Transmission and Intelligent Control,
Tianjin University of Technology, Tianjin 300384, China
[2]School of Materials Science and Engineering, Hebei University of Technology, Tianjin 300130, China

In this study, we propose Pt-modified InN (Pt-InN) as an adsorption and sensing material for typical SF$_6$ decomposition gases (SO$_2$, SOF$_2$, and SO$_2$F$_2$). On the basis of density functional theory, the adsorption structure, energy, charge transfer, deformed charge density, the total density of states, the partial density of states, and recovery time were discussed and calculated in detail, and the internal mechanism of the entire adsorption process was clarified. Analysis results show that Pt doping can considerably improve the characteristic response of pure InN monolayers to SF$_6$ decomposition gases. The high adsorption energy indicates a chemical interaction between the Pt-InN monolayer and SO$_2$, SOF$_2$, and SO$_2$F$_2$ molecules, making Pt-InN a potential candidate material for SF$_6$ decomposition gas sensors. This study also guides further research on InN as a gas sensor.

1. Introduction

Because SF$_6$ has strong electronegativity, excellent insulation performance, arc extinguishing ability, and good chemical stability, it is widely used in power systems for gas-insulated switchgear (GIS).[1,2] However, after the GIS has been working for a long time, there will inevitably be latent insulation defects inside, which usually lead to partial discharge. Under partial discharge, the insulating gas SF$_6$ inside the GIS will decompose to produce several low fluorine sulfides (SFx, x = 1–5) and F atoms.[3] Trace amounts of water and oxygen in the atmosphere can react with SFx to form various gases, mainly SO$_2$, SOF$_2$, SO$_2$F$_2$, and so on.[4–6] These compounds pollute the environment and significantly negatively impact SF$_6$'s insulation performance, leading to accidents, which means that detecting or removing these three dangerous gases is the key to the safe operation of SF$_6$ insulation devices.[7]

Indium nitride (InN) is a group III-V nitride.[8,9] The two-dimensional materials of III-V group compounds exhibit significant tunable bandgap and high stability and have a microstructure similar to that of graphene, which can be considered an analogue of graphene. Among them, InN monolayer films have a hexagonal geometry similar to graphene.

Theoretically, research has shown that InN monolayers have good sensitivity to gas molecules. Peng *et al.* indicated that Au-doped InN is a potential material for preparing SO_2, SOF_2, and SO_2F_2, as well as adsorbents and SOF_2 sensors.[10] In addition, Das and Yadav also studied the effects of cobalt modification on the electronic and vibrational properties of InN nanocages.[11] Sun *et al.* established a graphene-like InN in the N gas small molecule adsorption model.[12] Using first-principles calculations, they studied the adsorption behaviors of CO, NH_3, H_2S, NO_2, NO, and SO_2 gas small molecules on a monolayer in the N surface. Their results show that the sensitivity of InN to NH_3, SO_2, H_2S, and NO_2 is based on the varying degree of physical or chemical adsorption of small gas molecules. Single-layer InN materials have good application prospects in gas sensors. Research has found that doping the InN monolayer with transition metal atoms can enhance the adsorption capacity of gas molecules on the InN surface, and doping these transition metals can generate good electronic behaviors required for many electronic devices.[13] The development history of InN materials in gas sensing applications is very short. However, many experimental results have confirmed that two-dimensional InN monolayers have good thermal stability, high carrier mobility, good gas adsorption performance, and wide band gap.[11-13] Many literature reports have shown that two-dimensional single-layer materials exhibit excellent performance in gas sensor components, making research applying two-dimensional single-layer materials highly attractive.

In this study, we established and optimized an InN surface model and InN modified with catalytic metal Pt. The parameters related to the adsorption process of three SF_6 decomposition components (SO_2, SOF_2, and SO_2F_2) on the InN surface and Pt-InN crystal plane were calculated according to the first principles, which provide some theoretical guidance for exploring Pt-InN as a gas sensor used in the field of electrical engineering.

2.　Calculation Method

Density functional theory (DFT) was adopted for all simulation calculations, which were analyzed in the Dmol^3 module.[14,15] In this study, we used the exchange-related generalized gradient approximation (GGA) and the Perdew–Burke–Ernzerhof (PBE) functional to deal with the exchange crosslinking between electrons. Grimme dispersion correction was adopted. DFT Semicore Pseudopots (DSSP) were selected to replace the single nuclear electron effective potential. A double numeric basis with polarization functions (DNP) was chosen as the atomic orbital basis group.

A single-layer supercell model of 50 atoms of InN with periodic *x*- and *y*-axis boundary conditions was constructed to simulate infinite InN sheets. We set a vacuum layer of 20 Å $(1\,Å = 10^{-10}\,m)$ to avoid periodic interactions. After structural optimization, the lattice parameter of the InN monolayer was 3.62 Å, and the length of the In-N bond was 2.092 Å, consistent with previous reports.[16,17]

The energy convergence accuracy, maximum stress, and maximum displacement were set to 1×10^{-5} Ha (1 Ha = 27.212 eV), 2×10^{-3} Ha/Å, and 5×10^{-3} Å, respectively. We optimized the geometry of the k-point grid using $5 \times 5 \times 1$ and calculated the density of states (DOS) using $9 \times 9 \times 1$. We set the convergence accuracy of the self-consistent field to 1×10^{-6} Ha and the direct

inversion in the iterative subspace (DIIS) to 6, improving the convergence speed of the self-consistent field charge density, thus improving the efficiency.

The binding energy (E_b) formed by the interaction between Pt adsorption atoms and InN is obtained as[18–20]

$$E_b = E_{\text{Pt-InN}} - E_{\text{InN}} - E_{\text{Pt}}, \tag{1}$$

where $E_{\text{Pt-InN}}$ is the total energy of the Pt-modified InN, E_{InN} is the energy of intrinsic InN, and E_{Pt} is the energy of doped Pt atoms.

The adsorption energy of gas molecules on the InN surface is

$$E_{ads} = E_{Catalyst\text{-}gas} - E_{Catalyst} - E_{gas}. \tag{2}$$

Here, $E_{Catalyst\text{-}gas}$ is the total energy of the system after gas molecules are adsorbed onto the InN surface and E_{gas} is the energy of free gas. If the calculated adsorption energy is negative, it indicates that the adsorption process is exothermic and can occur spontaneously, showing that such a process is stable. The higher the absolute value of adsorption energy, the greater the change in total energy during the adsorption process, reflecting the stronger interaction between the sensing material and the adsorbed gas. We calculated and analyzed the charge transfer (Q_t) between gas molecules and Pt-modified InN structures by Hirshfeld charge analysis.

$$Q_t = Q_a - Q_b \tag{3}$$

3. Results and Analysis

3.1 Analysis of Pt-InN monolayer

A $5 \times 5 \times 1$ single-layer InN supercell model was constructed, as shown in Fig. 1(a). The band gap of the intrinsic InN crystal plane is 0.664 eV, and the length of the In-N bond is 2.092 Å. Metal doping on the InN crystal surface was studied. According to some domestic and international studies, Fig. 1(a) also shows the different local adsorption sites of the InN surface model, which represent the sites above the In atom, the positions above the N atom, the bridge positions between the In and N atoms, and the hollow centers on the hexagonal InN surface.[21] After geometric relaxation, by doping Pt at four different InN film positions, the Pt metal tends to move to the position above the N atom; this structure named Pt-InN is shown in Figs. 1(b) and 1(c). The binding energy of Pt-InN is −4.22 eV, the Pt-N bond length is 2.06 Å, and the band gap is 0.764 eV. From the top and front views of Pt-InN, the doping of Pt atoms slightly leads to the deformation of InN, providing a new gas adsorption site.

To fully understand the changes in the electronic behavior and conductivity of InN before and after Pt modification, spin-up and spin-down curves of the total density of states (TDOS) were established as shown in Fig. 2. Pt-InN TDOS generally shifts to the left, indicating increased
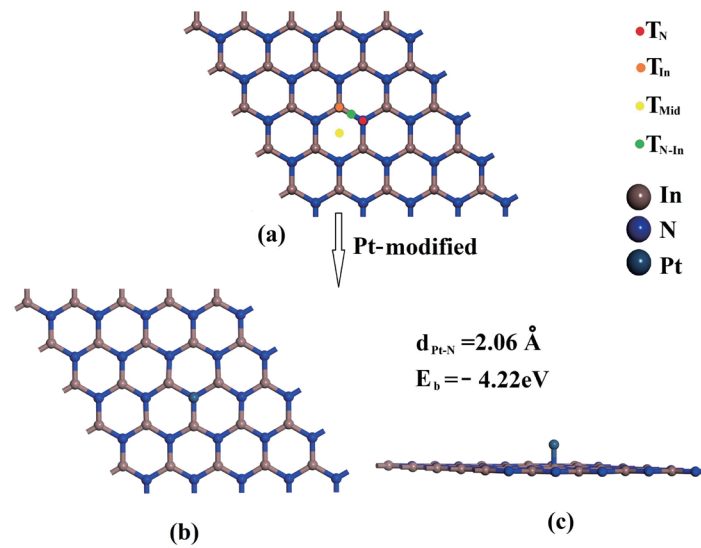
Fig. 1.   (Color online) Structure of Pt-modified InN: (a) four modified sites of InN, (b) top view of Pt-InN after modification, and (c) side view of Pt-InN.
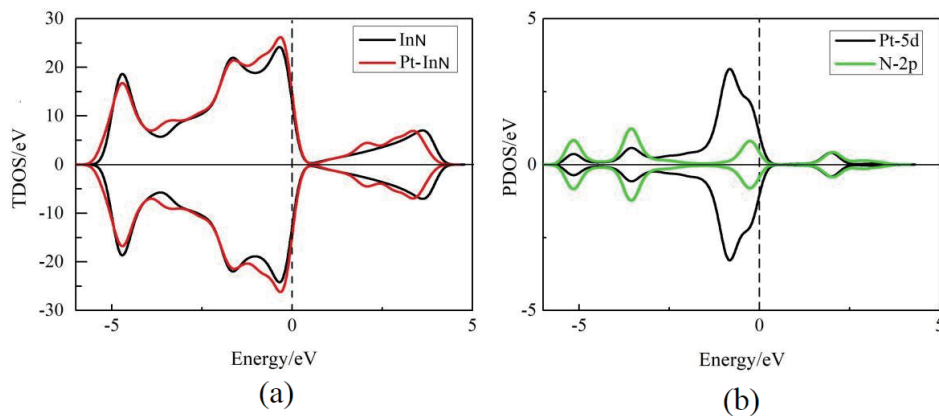
Fig. 2.   (Color online) TDOSs obtained before and after Pt doping of InN and PDOS of the main interacting atoms. (a) TDOS and (b) PDOS.

conductivity. Concerning the partial density of states (PDOS) curve, the N-2p orbit significantly overlaps with the Pt-5d orbit, which confirms that the N-2p and Pt-5d orbits exhibit strong hybridization, especially at the Fermi level. In addition, owing to the high symmetry of the spin-up and spin-down curves of TDOS, the InN monolayer is nonmagnetic. In summary, Pt-InN has a stable structure and enhanced conductivity, which may enhance SF_6 sensitivity to gas decomposition.

3.2   Adsorption of SF₆ decomposition gases on intrinsic InN surface

3.2.1   Adsorption model structure of SF₆ decomposition gas molecules on intrinsic InN

The structure of the adsorption model should be optimized to maximize microstructural parameters and approach basic physical and chemical standards. Figure 3(a) shows the optimal configuration of SO_2 adsorbed on the InN surface, where the S atom is located above the N atom, and the two O–S bonds are parallel to the two In-N bonds. Figure 3(a) also shows that the N atom of InN is close to the S atom of the gas molecule. In Table 1, except for the SO_2 adsorption system, the absolute E_{ad} values of the other two adsorption systems are below 0.8 eV, indicating that less energy is released or absorbed between gas molecules and crystal planes, leading to physical reactions. From the above analysis, it can be concluded that the adsorption detection effect of intrinsic InN on SF_6 decomposition components is minimal, as manifested by the low adsorption energy, large adsorption height, and small charge transfer.

3.2.2   Deformed charge density (DCD) analysis of SF₆ decomposition gases on intrinsic InN surface

To study the interactions of single SO_2, SOF_2, and SO_2F_2 gases adsorbed on the original InN surface, the DCD was analyzed. According to the DCDs of SO_2, SOF_2, and SO_2F_2 molecules adsorbed on the InN monolayer shown in Figs. 4(a)–4(c), respectively, the clear blue area shows electron loss. In contrast, the obvious red area shows electron capture. As shown in these DCDs, no obvious contact was found between the blue and red areas, so the interface interaction between the gas molecules of these three systems and the InN surface is unclear.
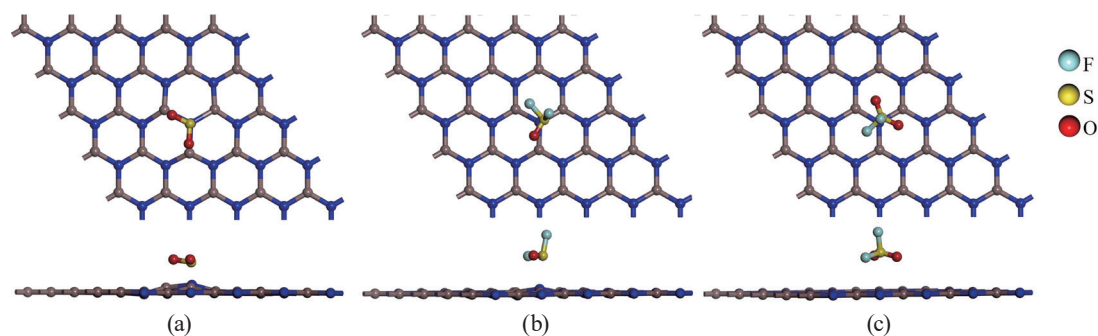
Fig. 3.   (Color online) Schematic of optimized structures of (a) SO_2, (b) SOF_2, and (c) SO_2F_2 on intrinsic InN surface.

Table 1
Q_T, adsorption distance (D), band gap (E_g), and adsorption energy (E_{ad}) values of SO_2, SOF_2, and SO_2F_2 on intrinsic InN.

Systems	Q_T (e)	D (Å)	E_g (eV)	E_{ad} (eV)
SO_2/InN	−0.309	1.770	0.737	−1.484
SOF_2/InN	−0.091	2.632	0.637	−0.530
SO_2F_2/InN	0.0256	3.183	0.635	−0.303
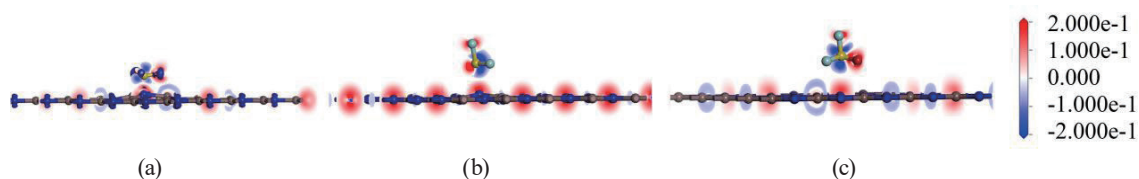
Fig. 4.   (Color online) DCDs of (a) SO_2, (b) SOF_2, and (c) SO_2F_2 molecules on InN.

3.3   Adsorption of SF_6 decomposition gases on Pt-InN surface

3.3.1   Absorption model structure of SF_6 decomposition gas molecules on Pt-InN

Figure 5(a) shows the stable adsorption model for SO_2 near Pt atoms on the Pt-InN layer, where Pt atoms adsorb S and O atoms in the SO_2 molecule. When the SO_2 adsorption system becomes stable, the characteristic adsorption parameters of the SO_2 adsorption model on the Pt-InN surface are calculated, as shown in Table 2. The closest distance between Pt atoms and SO_2 gas is 2.179 Å, and SO_2 molecules receive 0.225 e from Pt-InN. The E_{ad} of this adsorption system is approximately −1.642 eV, which means that there is adsorption energy between Pt-InN and SO_2.

Similarly, the optimal SOF_2 gas adsorption structure adsorbed on Pt-InN is shown in Fig. 5(b). The S atom in the SOF_2 molecule tends to be adsorbed by Pt, with an adsorption energy of −1.874 eV and an adsorption distance of 2.159 Å. Owing to the absolute value of the SOF_2 adsorption energy being greater than 0.8 eV, it can be determined that chemical adsorption occurs between SOF_2 and Pt-InN. According to Hirshfeld's analysis, Q_T in SOF_2 is −0.1264 e. SOF_2 acts as an electron acceptor, whereas Pt atoms act as a bridge to promote charge transfer between SOF_2 gas molecules and the Pt-InN surface, which is conducive to improving the gas sensing performance of Pt-InN sensors.

The optimal SO_2F_2 gas adsorption structure adsorbed on Pt-InN is shown in Fig. 5(c). The characteristic adsorption parameters of the SO_2F_2 adsorption model on the Pt-InN surface are calculated as shown in Table 2. The adsorption distance (2.202 Å), adsorption energy (−0.711 eV), and charge transfer (−0.1871 e) are displayed.

Table 3 shows the adsorption energies of SO_2, SOF_2, and SO_2F_2 gases on other two-dimensional materials. The Pt-modified InN monolayer membrane has moderate adsorption capacity for SO_2, SOF_2 and SO_2F_2 gases.

3.3.2   DCD and DOS analyses of SF_6 decomposition gases absorbed on Pt-InN surface

The DCDs of SO_2, SOF_2, and SO_2F_2 molecules adsorbed on the Pt-InN monolayer are shown in Figs. 6(a)–6(c), respectively. A viscous continuous electron region can be observed, indicating the electron transfer and adsorption of SO_2, SOF_2, and SO_2F_2 molecules on Pt-InN. To facilitate an understanding of the adsorption reactions of three SF_6 decomposition products on Pt-InN, the TDOSs and PDOSs of SF_6 decomposition products obtained before and after the adsorption
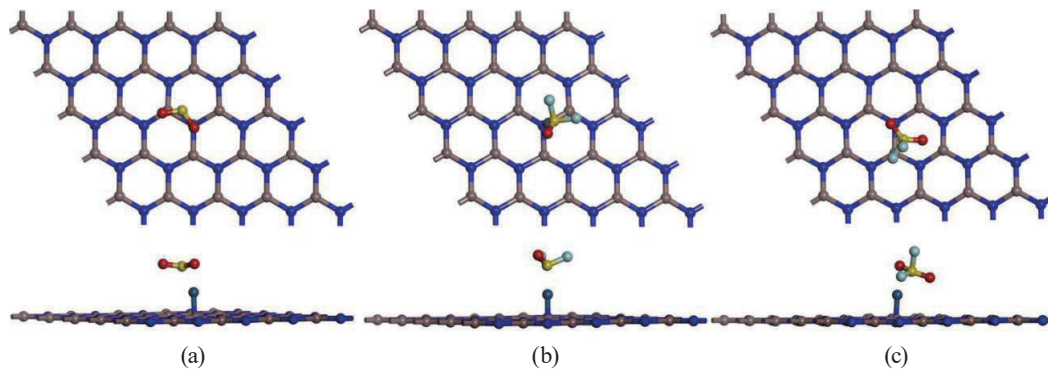
Fig. 5.　(Color online) Schematic of optimized structures of (a) SO_2, (b) SOF_2, and (c) SO_2F_2 on Pt-InN surface.

Table 2
Adsorption parameters of SO_2, SOF_2, and SO_2F_2 on Pt-InN.

Systems	Q_T (e)	D (Å)	E_g (eV)	E_{ad} (eV)
SO_2/Pt-InN	−0.2251	2.179	0.727	−1.642
SOF_2/Pt-InN	−0.1264	2.159	0.731	−1.874
SO_2F_2/Pt-InN	−0.1871	2.202	0.722	−0.711

Table 3
Comparison of adsorption energies for various materials.

Literature/gases	SO_2 (eV)	SOF_2 (eV)	SO_2F_2 (eV)
Pt-InN (this work)	−1.642	−1.874	−0.711
Co-GeSe[22]	−1.926	−1.223	−3.390
Cr-GeSe[22]	−3.125	−3.378	−3.803
FePc[23]	−1.09	−1.04	−0.29
MnPc[23]	−0.53	−0.57	0.36
Ag-GDY[24]	−1.583	−1.604	−1.905
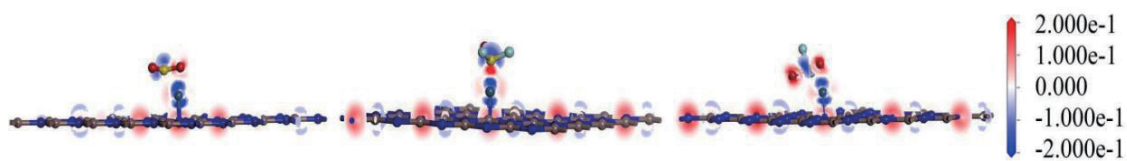
Fig. 6.　(Color online) DCDs of (a) SO_2, (b) SOF_2, and (c) SO_2F_2 molecules on Pt-InN.

system on Pt-InN were calculated, as shown in Fig. 7. The spin-up and spin-down curves are symmetrical, which verifies that SF_6 decomposition species on the adsorbed Pt-InN system are nonmagnetic. There is almost no difference between the main peaks observed before and after gas adsorption on the Pt-InN monolayer. Owing to the introduction of additional gas molecules, the TDOS curves of all gas adsorption systems tend to move toward the Fermi level.

　　As demonstrated by the SO_2 PDOS on the Pt-InN system in Figs. 7(a)–7(b), state overlaps can be observed in Pt-5d, O-2p, and S-3p, and they aggregate mainly at −7, −6.2, −4.3, −2, 1.5, and 2.7 eV positions, indicating that the doped system exhibits excellent geometrical stability during
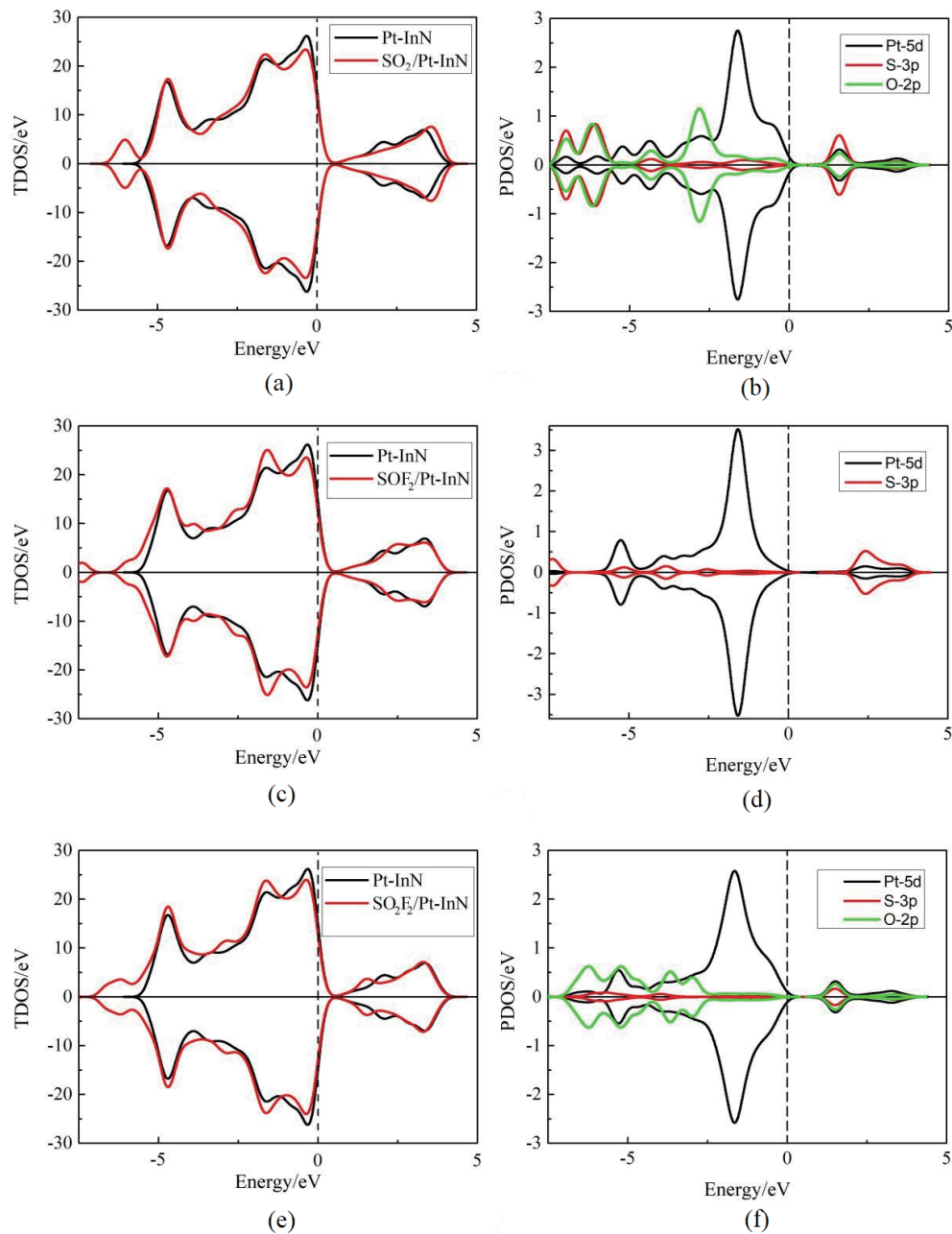
Fig. 7.   (Color online) TDOSs before and after gas adsorption and PDOS of the main interacting atoms in Pt-InN.

SO$_2$ adsorption. From Figs. 7(c)–7(d), it can be seen that Pt-5d orbitals exhibit peaks simultaneously with the S-3p orbitals at −4.3, −3.2, and 2 eV, indicating the chemical adsorption of SOF$_2$. As shown in Figs. 7(e)–7(f), it can be seen from the PDOS diagram that the Pt-5d orbit exhibits peaks at −4.2 and 2 eV simultaneously with the S-3p orbit. The number of overlapping peaks is relatively small, there is adsorption, and the adsorption energy is weak. In short, Pt-InN has a significantly higher adsorption stability for SF$_6$ decomposition gases than intrinsic InN.

3.3.3   Work function

The work function (Φ) was also calculated to explore further the adsorption behaviors of three gases on Pt-InN, as shown in Fig. 8. It defines the minimum energy required to move an electron from a Fermi level to infinity. The work function can be calculated as

$$\Phi = E_{Vac} - E_0 , \qquad (4)$$

where E_{Vac} and E_0 are the vacuum and Fermi potentials of the InN and Pt-InN systems, respectively. The intrinsic InN adsorption work functions for SO_2, SOF_2, and SO_2F_2 are 5.14, 5.06, and 4.98 eV, respectively. The Pt-InN adsorption work functions for SO_2, SOF_2, and SO_2F_2 are 5.17, 5.20, and 5.14 eV, respectively. The maximum work function occurs when SOF_2 adsorbs Pt-InN (5.20 eV); the calculated adsorption energy is also the highest. By introducing Pt decoration, different gas adsorption work functions were improved to varying degrees, indicating that the interaction between InN modified with Pt and the three gases was significantly enhanced, consistent with the corresponding adsorption and sensing.

3.3.4   Recovery time

Recovery time is an important parameter for gas sensors. A gas sensor must be repeatable, requiring its recovery time, i.e., the time for gas separation from sensitive media, to be relatively short. The recovery time can be obtained as

$$\tau = \omega^{-1} e^{\frac{-E_{ad}}{K_B T}} , \qquad (5)$$

where ω is a constant with a value of $\sim 10^{12}$ s^{-1}, E_{ad} is the adsorption energy, K_B represents the Boltzmann constant with a value of 8.62×10^{-5} eV/K, and T is temperature.

In accordance with Eq. (5), the recovery time for each adsorption curve is shown in Fig. 9. The recovery times of SO_2, SOF_2, and SO_2F_2 molecules on Pt-InN monolayers at several test temperatures (298, 398, 498, 598, and 698 K) were explained. The longitudinal comparison in Fig. 9 shows that as the temperature increases, the recovery time of the gas adsorption system decreases. However, when compared horizontally, the recovery time increases in the $SO_2F_2/SO_2/SOF_2$ order. At low operating temperatures of 298 and 398 K, it is difficult to desorb SO_2 and SOF_2 gases from Pt-InN monolayers. At 398 K, their desorption takes several years. This indicates that the material has great potential as a gas adsorbent to remove SO_2 and SOF_2 impurities in insulation equipment at low operating temperatures. However, under higher temperature conditions (598 K), the desorption time of SO_2 gas is only 67 s, and the desorption time of SOF_2 is still longer at this temperature. When heated to 698 K, the desorption of SOF_2 gas takes only 33 s, showing a good desorption effect. Conversely, at a room temperature of 298 K, the desorption of SO_2F_2 gas takes only 1.04 s. The short desorption time indicates that the Pt-InN monolayer can be used as an ideal sensing material for SO_2, SOF_2, and SO_2F_2 at different temperatures.
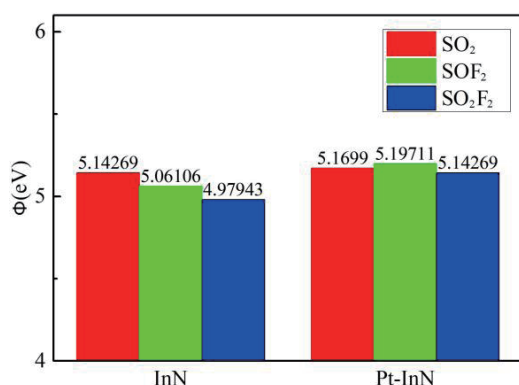
Fig. 8. (Color online) InN and Pt-InN work functions for SO_2, SOF_2, and SO_2F_2.
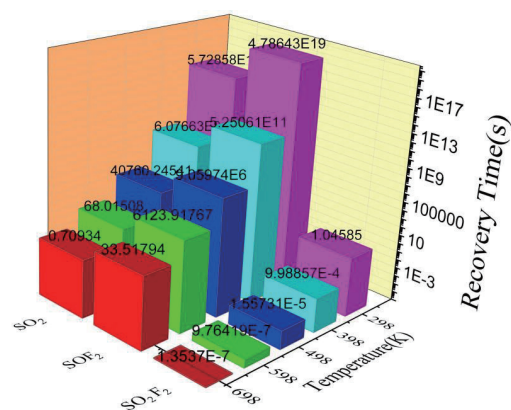
Fig. 9. (Color online) Recovery times for SF_6 decomposition components (SO_2, SOF_2, and SO_2F_2) at different temperatures.

4. Conclusions

The adsorption characteristics of SF_6 decomposition products on Pt-modified InN were systematically studied by first-principles calculations. The important conclusions of this study are summarized as follows.

The position of Pt above the N atom can be expressed as the best modified configuration of the Pt-modified hexagonal InN with high binding energy, which is considered the optimal system for studying adsorption performance. In addition, doping sites enhance the conductivity and electrochemical reactivity of the entire InN crystal surface.

Compared with the intrinsic InN adsorption system, the gas molecules SO_2, SOF_2, and SO_2F_2 adsorbed on Pt-InN exhibit ideal chemical adsorption effects owing to the high adsorption energy and strong overlapping peaks in PDOS. Given the desorption time, using the Pt-InN monolayer as a potential gas sensing material for detecting SF_6 decomposition products makes sense.

References

1   D. Chen, X. Zhang, J. Tang, Y. Li, Z. Cui, and Q. Zhou: IEEE Trans. Electron Devices **66** (2019) 689. http://doi.org/10.1109/TED.2018.2882236
2   J. Tang, F. Liu, X. Zhang, Q. Meng, and J. Zhou: IEEE Trans. Dielectr. Electr. Insul. **19** (2012) 29. http://doi.org/10.1109/TDEI.2012.6148499
3   X. Zhang, L. Yu, Y. Gui, and W. Hu: Appl. Surf. Sci. **367** (2016) 259. https://doi.org/10.1016/j.apsusc.2016.01.168
4   H. Cui, T. Liu, Y. Zhang, and X. Zhang: IEEE Sens. J. **19** (2019) 5249. http://doi.org/10.1109/JSEN.2019.2899966
5   Y. Fu, M. Rong, K. Yang, A. Yang, X. Wang, Q. Gao, D. Liu, and A. B. Murphy: J. Phys. D: Appl. Phys. **49** (2016) 155502. http://doi.org/10.1088/0022-3727/49/15/155502
6   P. Xu, Y. Gui, and X. Chen: Diamond Relat. Mater. **126** (2022) 109103. https://doi.org/10.1016/j.diamond.2022.109103
7   D. Wang, X. Wang, A. Yang, J. Chu, P. Lv, Y. Liu, and M. Rong: IEEE Electron Device Lett. **39** (2018) 292. http://doi.org/10.1109/LED.2017.2786322

8 C. Bungaro, K. Rapcewicz, and J. Bernholc: Phy. Rev. B **61** (2000) 6720. http://doi.org/10.1103/PhysRevB.61.6720

9 S. Pi, T. Yang, Q. Zhang, and Y. Liu: Comput. Theor. Chem. **1206** (2021) 113479. http://doi.org/https://doi.org/10.1016/j.comptc.2021.113479

10 R. Peng, Q. Zhou, and W. Zeng: Nanomaterials **11** (2021) 1708. https://doi.org/10.3390/nano11071708

11 A. Das and R. K. Yadav: Comput. Theor. Chem. **1205** (2021) 113447. https://doi.org/10.1016/j.comptc.2021.113447

12 X. Sun, Q. Yang, R. Meng, C. Tan, Q. Liang, J. Jiang, H. Ye, and X. Chen: Appl. Surf. Sci. **404** (2017) 291. https://doi.org/10.1016/j.apsusc.2017.01.264

13 Y. Guo, Y. Zhang, W. Wu, Y. Liu, and Z. Zhou: Appl. Surf. Sci. **455** (2018) 106. https://doi.org/10.1016/j.apsusc.2018.05.116

14 K. Ghosh, H. Ma, V. Gavini, and G. Galli: Phys. Rev. Mater. **3** (2019) 043801. http://doi.org/10.1103/PhysRevMaterials.3.043801

15 D. Wu, L. Zhou, C. Chen, and X. Liang: Sens. Mater. **35** (2023). http://doi.org/10.18494/sam4079

16 J. Ben, X. Liu, C. Wang, Y. Zhang, Z. Shi, Y. Jia, S. Zhang, H. Zhang, W. Yu, D. Li, and X. Sun: Adv. Mater. **33** (2021) 2006761. https://doi.org/10.1002/adma.202006761

17 Y. Liu, Q. Zhou, B. Li, and W. Zeng: IEEE Sens. J. **21** (2021) 26586. http://doi.org/10.1109/JSEN.2021.3123283

18 R. Gao, Y. Yong, S. Hu, Z. Zhao, X. Li, and Y. Kuang: Appl. Surf. Sci. **568** (2021) 150961. https://doi.org/10.1016/j.apsusc.2021.150961

19 M. Isa Khan, I. Ashfaq, A. Majid, M. Shakil, and N. ul ain: Mater. Chem. Phys. **295** (2023) 127174. https://doi.org/10.1016/j.matchemphys.2022.127174

20 Q. Li, D. Chen, Y. Liu, J. Miao, C. Zhang, X. Chen, and D. Cui: Surf. Interfaces **36** (2023) 102514. https://doi.org/10.1016/j.surfin.2022.102514

21 Y. Liao, Q. Zhou, W. Hou, J. Li, and W. Zeng: Appl. Surf. Sci. **561** (2021) 149816. http://doi.org/https://doi.org/10.1016/j.apsusc.2021.149816

22 J. Chen, L. Jia, X. Cui, W. Zeng, and Q. Zhou: Mater. Today Chem. **28** (2023) 101382. https://doi.org/10.1016/j.mtchem.2023.101382

23 Z. Nie, C. Wang, R. Xue, G. Xie, and H. Xiong: Appl. Surf. Sci. **608** (2023) 155119. https://doi.org/10.1016/j.apsusc.2022.155119

24 R. Wang, B. Cheng, and W. Ou: Appl. Surf. Sci. **608** (2023) 155276. https://doi.org/10.1016/j.apsusc.2022.155276

About the Authors

Youjun Yue received his B.S. degree from Tianjin University of Technology, China, in 1993, and his M.S. and Ph.D. degrees from Tianjin University, China, in 2000 and 2010, respectively. Currently, he is a professor at Tianjin University of Technology. His research interests are in the fault diagnosis of insulation equipment and the modeling of complex systems in process industry. (bakeryue@tjut.edu.cn)

Guilin Chen received his bachelor's degree from Henan Polytechnic University in 2022 and has been pursuing a graduate degree at Tianjin University of Technology since 2023. His research interests are in the fault diagnosis of insulation equipment and computer simulation. (2583599768@qq.com)

Dongyue Wu received his B.S. degree from Hebei University of Technology, China, in 2005, and his M.S. and Ph.D. degrees from Tianjin University, China, in 2008 and 2012, respectively. Since 2012, he has been a lecturer at Tianjin University of Technology, China. His research interests are in multisensor fusion, detection signal analysis, and the fault diagnosis of processing and insulation equipment. (tsam0925@163.com)

Linxi Zhou received her B.S. degree from Hebei Normal University, China, in 2005 and her M.S. degree from Nankai University, China, in 2009. Since 2011, she has been a researcher at Hebei University of Technology, China. Her research interests are in the synthesis, preparation, and performance research of materials. (zhoulinxi@hebut.edu.cn)

Yiliduosi Zupaer has been an undergraduate student at Tianjin University of Technology since 2021. His research interest is in the fault diagnosis of insulation equipment. (3154891782@qq.com)